

# A Generalised Gaussian Extension to the Rician Distribution for Modelling SAR Imagery

Oktay Karakuş, *Member, IEEE*, Ercan E. Kuruoglu, *Senior Member, IEEE*, Alin Achim, *Senior Member, IEEE*

**Abstract**—In this paper, we present a novel statistical model, the generalised-Gaussian-Rician (GG-Rician) distribution, for the characterisation of synthetic aperture radar (SAR) images. Since accurate statistical models lead to better results in applications such as target tracking, classification, or despeckling, characterising SAR images of various scenes including urban, sea surface, or agricultural, is essential. The proposed statistical model is based on the Rician distribution to model the amplitude of a complex SAR signal, the in-phase and quadrature components of which are assumed to be generalised-Gaussian distributed. The proposed amplitude GG-Rician model is further extended to cover the intensity SAR signals. In the experimental analysis, the GG-Rician model is investigated for amplitude and intensity SAR images of various frequency bands and scenes in comparison to state-of-the-art statistical models that include  $\mathcal{K}$ , Weibull, Gamma, and Lognormal. In order to decide on the most suitable model, statistical significance analysis via Kullback-Leibler divergence and Kolmogorov-Smirnov statistics are performed. The results demonstrate the superior performance and flexibility of the proposed model for all frequency bands and scenes, and its applicability on both amplitude and intensity SAR images.

**Index Terms**—SAR amplitude modelling, SAR intensity modelling, Non-Gaussian scattering, generalised-Gaussian-Rician distribution.

## I. INTRODUCTION

**S**YNTHETIC aperture radar (SAR) imagery is an essential source of information in the analysis of various terrains thanks to its capability to capture wider areas under different weather conditions. Statistical modelling of SAR images plays an essential role in characterising various scenes and underpins applications such as classification [1], [2], denoising [3], [4]. The literature abounds with numerous statistical models for different SAR scenes, which are either theoretical or empirical, and all these models have some advantages and disadvantages according to the scene and/or frequency band changes.

In this paper, we address the problem of accurately modelling the SAR amplitude/intensity data within the context of probability density function (pdf) estimation by assuming the back-scattered SAR signal components possess heavy-tailed and/or non-Gaussian nature. Specifically, we aim to propose a generic and flexible statistical model in order to cover various different characteristics of the back-scattered SAR signal,

This work was supported by the UK Engineering and Physical Sciences Research Council (EPSRC) under grant EP/R009260/1 (AssenSAR).

Oktay Karakuş and Alin Achim are with the Visual Information Laboratory, University of Bristol, Bristol BS1 5DD, U.K. (e-mail: o.karakus@bristol.ac.uk; alin.achim@bristol.ac.uk)

Ercan E. Kuruoglu is with Data Science and Information Technology Center, Tsinghua-Berkeley Shenzhen Institute, China and is on leave from ISTI-CNR, Pisa, Italy. (e-mail: ercan.kuruoglu@isti.cnr.it)

and to address a robust statistical model potentially for the applications such as despeckling, classification, segmentation.

The standard SAR signal model defines the back-scattered SAR signal received by a SAR sensor as a complex signal  $R = x + iy$ , where  $x$  and  $y$  are the real and imaginary parts, respectively and follows several assumptions [5], [6]:

- 1) The number of scatterers is large,
- 2) The scatterers are statistically independent,
- 3) The instantaneous scattering phases are statistically independent of the amplitudes,
- 4) The phase is uniformly distributed,
- 5) The reflectors are relatively small when compared to the illuminated scene,
- 6) There is no dominating scatterer in the scene.

In particular, the first two assumptions recall the central limit theorem whereby the real and imaginary parts are jointly Gaussian. Combining with the assumption 6, this leads to the case where  $x$  and  $y$  are independent and identically distributed (i.i.d.) zero-mean Gaussian random variables,

$$x \sim \mathcal{N}(0, \sigma^2) \quad \text{and} \quad y \sim \mathcal{N}(0, \sigma^2). \quad (1)$$

Thence, the amplitude distribution becomes the *Rayleigh* distribution, the probability density function (pdf) of which is given by

$$f(r|\sigma) = \frac{r}{\sigma^2} \exp\left(-\frac{r^2}{2\sigma^2}\right) \quad (2)$$

where  $r = \sqrt{x^2 + y^2}$  refers to the amplitude with phase  $\theta = \arctan(x/y)$ , and  $\sigma$  is the scale parameter.

In cases when the illuminated scene includes a dominating scatterer, where the assumption 6 is no longer valid,  $x$  and  $y$  become identically and independent, but this time non-zero-mean ( $\delta$ ) Gaussian random variables as

$$x \sim \mathcal{N}(\delta, \sigma^2) \quad \text{and} \quad y \sim \mathcal{N}(\delta, \sigma^2). \quad (3)$$

where  $\delta > 0$  is the non-zero mean of components  $x$  and  $y$  [7]. Hence, the amplitude distribution follows the *Rician* distribution with pdf given by

$$f(r|\gamma, \Delta) = \frac{r}{\sigma^2} \exp\left(-\frac{r^2 + \Delta^2}{2\sigma^2}\right) \mathcal{I}_0\left(\frac{r\Delta}{\sigma^2}\right) \quad (4)$$

where  $\Delta$  is the location parameter,  $\mathcal{I}_0(\cdot)$  refers to the zeroth-order modified Bessel function of the first kind.

Even though they are theoretically appealing and analytically simple, Gaussian/Rayleigh based statistical models do not reflect the real life phenomena in most cases for SAR reflections. Thus, there are numerous statistical models in

the literature which were developed to account for non-Rayleigh cases, and proven to be successful for modelling SAR imagery. Among those, the  $\mathcal{K}$  distribution [8]–[10] is one of the important statistical models for both modelling the amplitude and intensity SAR images. The  $\mathcal{K}$  distribution pdf for amplitude modelling is expressed as

$$f(r|\alpha, \gamma) = \frac{2}{\gamma \Gamma(\alpha + 1)} \left( \frac{r}{2\gamma} \right)^{\alpha+1} K_\alpha \left( \frac{r}{\gamma} \right) \quad (5)$$

where  $\alpha$  and  $\gamma$  refer to the shape, and scale parameters, respectively. The Gamma distribution is another important statistical model for characterising multi look SAR intensity images [8], [11]. It is the generalisation of the exponential distribution via averaging  $L$  single-look SAR intensities, each of which are exponentially distributed. The pdf expression for the Gamma distribution is given as

$$f(\nu|L, \gamma) = \frac{(\gamma L)^L}{\Gamma(L)} \nu^{L-1} \exp(-\gamma L\nu), \quad (6)$$

where  $\nu = r^2$  is the intensity SAR signal,  $\gamma$  is the scale parameter and  $\Gamma(\cdot)$  refers to the Gamma function.

Contrary to the theoretical models discussed above, the Weibull distribution is an empirical statistical model, and has been used in the literature [10], [12], [13] to model SAR images of both amplitude and intensity. The Weibull pdf is expressed as

$$f(r|\alpha, \gamma) = \frac{\alpha}{\gamma} \left( \frac{r}{\gamma} \right)^{\alpha-1} \exp \left( - \left( \frac{r}{\gamma} \right)^\alpha \right) \quad (7)$$

where  $\alpha$  refers to the shape parameter, and  $\gamma$  is the scale parameter. The Lognormal distribution is another empirical model like Weibull and generally been used to model SAR amplitude [14], [15]. The lognormal pdf expression is

$$f(r|\mu, \gamma) = \frac{1}{r\gamma\sqrt{2\pi}} \exp \left( - \frac{(\log r - \mu)^2}{2\gamma^2} \right) \quad (8)$$

where  $\gamma$  is the scale, and  $\mu$  is the location parameter.

In a previous study, following the observation of non-Gaussian reflections in urban areas, Kuruoglu & Zerubia [5] have proposed a generalised central limit theorem based statistical model which extends the standard scattering model discussed above by addressing the real and the imaginary parts of the complex back-scattered SAR signal as jointly symmetric- $\alpha$ -Stable random variables. This model, called the generalised Rayleigh distribution (will be denoted as Stable-Rayleigh, or shortly SR for the rest of the paper) for amplitude SAR images, the pdf of which is given as

$$f(r|\alpha, \gamma) = r \int_0^\infty s \exp(-\gamma s^\alpha) \mathcal{J}_0(sr) ds \quad (9)$$

where  $\alpha$  and  $\gamma$  refer to the shape, and scale parameters, respectively. SR has been shown to be a good choice for urban SAR image modelling in [5], [16] and successfully applied to despeckling problem in [3].

Moser et, al, [6] have proposed another generalised theoretical statistical model for amplitude SAR modelling, which is similar to SR [5], by assuming the real and imaginary parts of the back-scattered signal to be independent zero-mean

generalised Gaussian (GG) random variables, which leads to the generalised Gaussian Rayleigh (GGR) distribution, with the pdf [6]

$$f(r|\alpha, \gamma) = \frac{\alpha^2 r}{4\gamma^2 \Gamma^2(\frac{1}{\alpha})} \times \int_0^{2\pi} \exp \left( - \frac{|r \cos \theta|^\alpha + |r \sin \theta|^\alpha}{\gamma^\alpha} \right) d\theta \quad (10)$$

where  $\alpha$  and  $\gamma$  refer to the shape, and scale parameters, respectively.

In a recent study [17], we have proposed a novel statistical model, namely the *Laplace-Rician* distribution for modelling amplitude SAR images of the sea surface. The Laplace-Rician model is based on the Rician distribution, whereby we assume that the real and imaginary parts of the back-scattered SAR signal are non-zero mean Laplace distributed. The Rician distribution is widely used in SAR imagery applications, and in the literature, it has a special importance in characterising SAR scenes with many strong back-scattered echoes from some natural targets such as forest canopy, mountain tops, sea waves, and some man-made structures with dihedral or trihedral configurations such as buildings, vessels [7], [18]–[23]. Combining the Rician idea with the non-Gaussian case via Laplace distribution in [17] addresses both the non-Rayleigh and heavy-tailed characteristics of amplitude SAR images. The Laplace-Rician model, despite being limited to a Laplace distribution as the backscattered SAR signal components' statistical model, showed superior performance for modelling amplitude SAR images of the sea surface when compared to the state-of-the-art statistical models such as Weibull, lognormal, and  $\mathcal{K}$  [17].

In this paper, we propose a novel statistical model by extending the Laplace-Rician model into a complete general case, where the back-scattered SAR signal components are *non-zero mean Generalised-Gaussian* distributed. We further propose a Markov chain Monte Carlo (MCMC) based Bayesian parameter estimation method for the proposed statistical model, and demonstrate the modelling capability of the proposed statistical model for amplitude/intensity SAR images from satellite platforms, TerraSAR-X, ICEYE, COSMO/Sky-Med, Sentinel-1 and ALOS2, and for illuminated scenes of urban, agricultural, land cover, sea surface with and without ships, along with several mixed scenes. We evaluate the performance of the proposed statistical model in a comparison study to the state-of-the-art statistical models of  $\mathcal{K}$ , Rayleigh, Rician, Gamma, Weibull, Lognormal, SR [5], and GGR [6].

The rest of the paper is organised as follows: we present the proposed statistical model in Section II. The Bayesian parameter estimation method is presented in III, whilst the experimental analysis is demonstrated in Section IV. Section V concludes the paper by remarks and future work.

## II. GENERALISED GAUSSIAN RICIAN MODEL

As mentioned above, in this paper, we propose a general statistical model, which is the extension of the generalised-Gaussian distribution into the Rician scattering idea. Our derivation starts by assuming that the illuminated SAR scene

includes one (or more) dominating scatterers, such as vehicles, buildings, sea waves. Following this, the sixth assumption given above for the back-scattered SAR signal, which is "There is no dominating scatterer in the scene." will not be valid anymore. Then, as in the Rician case, the real and imaginary components of the back-scattered complex SAR signal will be non-zero mean random variables.

We then recall the generalised Gaussian pdf

$$f(x|\alpha, \gamma, \delta) = \frac{\alpha}{2\gamma\Gamma(\frac{1}{\alpha})} \exp\left(-\left|\frac{x-\delta}{\gamma}\right|^\alpha\right), \quad (11)$$

where  $\delta$  is the location parameters. In order to have a Rayleigh-type amplitude distribution, the location parameter  $\delta$  is assumed to be zero, where the assumption 6 is valid. However, for the non-zero  $\delta$ , as long as the complex SAR signal components  $x$  and  $y$  are independent [6], the joint pdf can be written as

$$f(x, y|\alpha, \gamma, \delta) = f(x|\alpha, \gamma, \delta) \times f(y|\alpha, \gamma, \delta) \quad (12)$$

$$= \frac{\alpha}{2\gamma\Gamma(\frac{1}{\alpha})} \exp\left(-\left|\frac{x-\delta}{\gamma}\right|^\alpha\right) \times \frac{\alpha}{2\gamma\Gamma(\frac{1}{\alpha})} \exp\left(-\left|\frac{y-\delta}{\gamma}\right|^\alpha\right) \quad (13)$$

$$= \frac{\alpha^2}{4\gamma^2\Gamma^2(\frac{1}{\alpha})} \exp\left(-\frac{|x-\delta|^\alpha + |y-\delta|^\alpha}{\gamma^\alpha}\right). \quad (14)$$

Then, the amplitude distribution can be written by using the identity,  $f(r, \theta) = rf(r \cos \theta, r \sin \theta)$ , as

$$f(r, \theta|\alpha, \gamma, \delta) = r \frac{\alpha^2}{4\gamma^2\Gamma^2(\frac{1}{\alpha})} \times \exp\left(-\frac{|r \cos \theta - \delta|^\alpha + |r \sin \theta - \delta|^\alpha}{\gamma^\alpha}\right). \quad (15)$$

Hence, the corresponding marginal amplitude pdf can be obtained by averaging (15) over  $\theta$  and boils down to:

$$f(r|\alpha, \gamma, \delta) = \frac{\alpha^2 r}{4\gamma^2\Gamma^2(\frac{1}{\alpha})} \times \int_0^{2\pi} \exp\left(-\frac{|r \cos \theta - \delta|^\alpha + |r \sin \theta - \delta|^\alpha}{\gamma^\alpha}\right) d\theta, \quad (16)$$

The integral form pdf expression shown in (16) refers to the proposed statistical model for the amplitude distribution of a complex back-scattered SAR signal, the components of which are non-zero mean generalised-Gaussian distributed. Then, we note the theorems below.

**Theorem 1.** *The pdf expression given in (16) reduces to the Rician distribution in (4) for  $\alpha = 2$ , where the real and imaginary components of back-scattered SAR signal become non-zero mean Gaussian random variables.*

*Proof.* Starting from (16), and we set the shape parameter  $\alpha = 2$ , we have

$$f(r|\alpha = 2, \gamma, \delta) = \frac{r}{\gamma^2\pi} \times \int_0^{2\pi} \exp\left(-\frac{(r \cos \theta - \delta)^2 + (r \sin \theta - \delta)^2}{\gamma^2}\right) d\theta, \quad (17)$$

$$= \frac{r}{\gamma^2\pi} \times \int_0^{2\pi} \exp\left(-\frac{r^2 - 2r\delta(\cos \theta + \sin \theta) + 2\delta^2}{\gamma^2}\right) d\theta, \quad (18)$$

$$= \frac{r}{\gamma^2\pi} \exp\left(-\frac{r^2 + 2\delta^2}{\gamma^2}\right) \times \int_0^{2\pi} \exp\left(\frac{r\delta(\cos \theta + \sin \theta)}{\gamma^2/2}\right) d\theta, \quad (19)$$

Using the identity

$$(\cos \theta + \sin \theta) = \sqrt{2} \cos(\theta - \pi/4), \quad (20)$$

we have

$$f(r|\gamma, \delta) = \frac{r}{\gamma^2\pi} \exp\left(-\frac{r^2 + 2\delta^2}{\gamma^2}\right) \times \int_0^{2\pi} \exp\left(\frac{r\sqrt{2}\delta \cos(\theta - \pi/4)}{\gamma^2/2}\right) d\theta. \quad (21)$$

Recall that the zeroth order modified Bessel function of the first kind is expressed as

$$\mathcal{I}_0(z) = \frac{1}{2\pi} \int_0^{2\pi} \exp(z \cos \theta) d\theta. \quad (22)$$

After basic modifications we can express the pdf as

$$f(r|\gamma, \delta) = \underbrace{\frac{2\pi r}{\gamma^2\pi} \exp\left(-\frac{r^2 + 2\delta^2}{\gamma^2}\right)}_{\mathcal{I}_0\left(\frac{r\sqrt{2}\delta}{\gamma^2/2}\right)} \underbrace{\frac{1}{2\pi} \int_0^{2\pi} \exp\left(\frac{r\sqrt{2}\delta \cos(\theta - \pi/4)}{\gamma^2/2}\right) d\theta}_{\mathcal{I}_0\left(\frac{r\sqrt{2}\delta}{\gamma^2/2}\right)}. \quad (23)$$

It is straightforward to see that the integral on the right hand side is basically a zeroth order modified Bessel function of the first kind, then we have

$$f(r|\gamma, \delta) = \frac{r}{\gamma^2/2} \exp\left(-\frac{r^2 + 2\delta^2}{\gamma^2}\right) \mathcal{I}_0\left(\frac{r\sqrt{2}\delta}{\gamma^2/2}\right), \quad (24)$$

which is the Rician distribution for  $\gamma^2/2 = \sigma^2$  and  $\sqrt{2}\delta = \Delta$  in (4).  $\square$

**Theorem 2.** *The pdf expression given in (16) is the Laplace-Rician distribution [17] for  $\alpha = 1$ ,*

$$f(r|\gamma, \delta) = \frac{r}{4\gamma^2} \int_0^{2\pi} \exp\left(-\frac{|r \cos \theta - \delta| + |r \sin \theta - \delta|}{\gamma}\right) d\theta. \quad (25)$$

where real and imaginary components of back-scattered SAR signal are distributed non-zero mean Laplace distribution.

*Proof.* For the proof of the Theorem 2, we refer the reader to [17].  $\square$

**Remark 1.** *We refer to the proposed pdf expression in (16) as the generalised Gaussian-Rician distribution (GG-Rician), since it extends the Rician amplitude model to a heavy tailed*

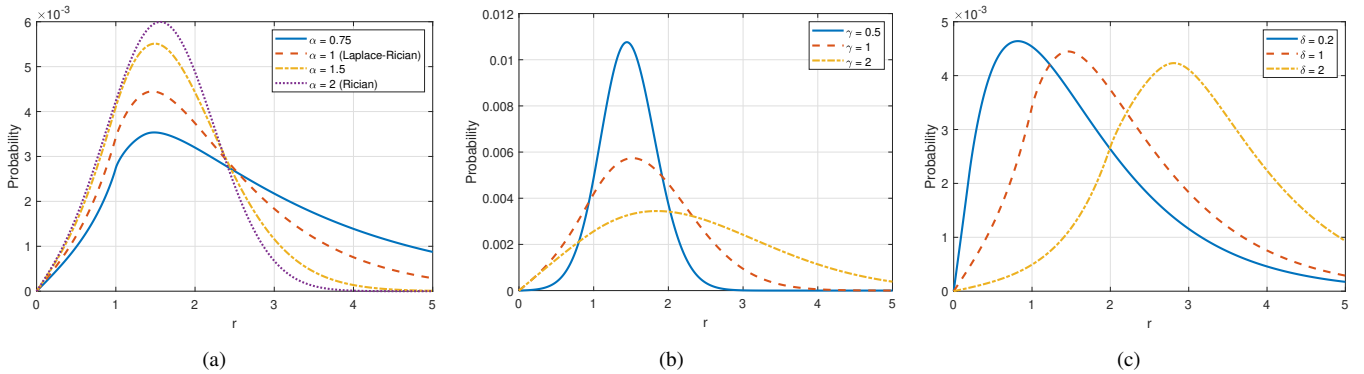


Fig. 1. The proposed GG-Rician distribution pdfs for different model parameters of (a) the shape parameter  $\alpha$  ( $\gamma = 1$  and  $\delta = 1$ ), (b) the scale parameter  $\gamma$  ( $\alpha = 1.7$  and  $\delta = 1$ ), and (c) the location parameter  $\delta$  ( $\alpha = 1$  and  $\gamma = 1$ ).

context via the generalised Gaussian distributed complex SAR signal components.

To give a feeling for the characteristics of this class of distributions, they are plotted for various values of the parameters in Figure 1.

#### A. Extension to Intensity SAR Images

The derived proposed statistical model (16) characterises the amplitude SAR signal. However, for some applications, intensity SAR images have been used instead of amplitude images. In this section, we derive the intensity pdf expression for the proposed GG-Rician statistical model.

For an intensity SAR image, the pdf expression can be calculated from the pdf of the amplitude image using the pdf transformation formula:

$$f_I(\nu) = \frac{1}{2\nu} f_A(\sqrt{\nu}) \quad (26)$$

where  $\nu = r^2$  refers to the intensity with the pdf of  $f_I(\cdot)$ . Then, using the identity in (26), the GG-Rician intensity pdf can be given as

$$f_I(\nu|\alpha, \gamma, \delta) = \frac{\alpha^2}{8\gamma^2 \Gamma^2(\frac{1}{\alpha})} \times \int_0^{2\pi} \exp\left(-\frac{|\sqrt{\nu} \cos \theta - \delta|^\alpha + |\sqrt{\nu} \sin \theta - \delta|^\alpha}{\gamma^\alpha}\right) d\theta. \quad (27)$$

**Theorem 3.** The intensity pdf expression given in (27) simplifies to the Nakagami-Rice distribution [1], [24] for  $\alpha = 2$

$$f_I(\nu|R, \Delta) = \frac{1}{R} \exp\left(-\frac{\nu + \Delta^2}{R}\right) \mathcal{I}_0\left(\frac{\sqrt{\nu \Delta^2}}{R/2}\right) \quad (28)$$

where  $R$  is the scale and  $\Delta$  is the location parameter.

*Proof.* We start by recalling (27), and setting the shape parameter  $\alpha = 2$ . Then, we have

$$f_I(\nu|\alpha = 2, \gamma, \delta) = \frac{1}{2\gamma^2 \pi} \times \int_0^{2\pi} \exp\left(-\frac{|\sqrt{\nu} \cos \theta - \delta|^2 + |\sqrt{\nu} \sin \theta - \delta|^\alpha}{\gamma^2}\right) d\theta. \quad (29)$$

$$= \frac{1}{2\gamma^2 \pi} \times \int_0^{2\pi} \exp\left(-\frac{\nu - 2\sqrt{\nu}\delta(\cos \theta + \sin \theta) + 2\delta^2}{\gamma^2}\right) d\theta. \quad (30)$$

$$= \frac{1}{2\gamma^2 \pi} \exp\left(-\frac{\nu + 2\delta^2}{\gamma^2}\right) \int_0^{2\pi} \exp\left(\frac{\sqrt{\nu}\delta(\cos \theta + \sin \theta)}{\gamma^2/2}\right) d\theta. \quad (31)$$

In a way akin to the proof of Theorem 1, we can easily write the expression in (31) as

$$f_I(\nu|\gamma, \delta) = \frac{2\pi}{2\gamma^2 \pi} \exp\left(-\frac{\nu + 2\delta^2}{\gamma^2}\right) \times \underbrace{\frac{1}{2\pi} \int_0^{2\pi} \exp\left(\frac{\sqrt{\nu}\delta}{\gamma^2/2} \cos(\theta - \pi/4)\right) d\theta}_{\mathcal{I}_0\left(\frac{\sqrt{\nu}\delta^2}{\gamma^2/2}\right)}. \quad (32)$$

It is straightforward to see that the integral on the right hand side is basically a zeroth order modified Bessel function of the first kind, then we have

$$f_I(\nu|\gamma, \delta) = \frac{1}{\gamma^2} \exp\left(-\frac{\nu + 2\delta^2}{\gamma^2}\right) \mathcal{I}_0\left(\frac{\sqrt{\nu}\delta^2}{\gamma^2/2}\right), \quad (33)$$

which is the Nakagami-Rician distribution for  $\gamma^2 = R$  and  $2\delta^2 = \Delta^2$ , and completes the proof.  $\square$

**Remark 2.** It is straightforward to state that for  $\alpha = 2$  and  $\delta = 0$ , with a derivation akin to Theorem 3, the corresponding intensity pdf will boil down to the **exponential distribution**, and similarly for L-look case to the **Gamma distribution**.

As mentioned up to this point, the GG-Rician statistical model is a general statistical model, which covers various important amplitude and intensity statistical models as special members. For the completeness, we share GG-Rician pdf expressions, and some special cases in Table I.

TABLE I  
GG-RICIAN FAMILY SPECIAL MEMBERS FOR AMPLITUDE AND INTENSITY.

Distribution	Expression
GG-Rician (Amplitude)	$f(r \alpha, \gamma, \delta)$ in (16)
Rayleigh	$f(r 2, \gamma, 0)$
Rician	$f(r 2, \gamma, \delta)$
GGR [6]	$f(r \alpha, \gamma, 0)$
Nakagami	$L$ -look average of $f(r 2, \gamma, 0)$
Laplace-Rician [17]	$f(r 1, \gamma, \delta)$
GG-Rician (Intensity)	$f_I(\nu \alpha, \gamma, \delta)$ in (27)
Exponential	$f_I(\nu 2, \gamma, 0)$
Nakagami-Rice	$f_I(\nu 2, \gamma, \delta)$
Gamma	$L$ -look average of $f_I(\nu 2, \gamma, 0)$

### III. BAYESIAN PARAMETER ESTIMATION METHOD

Since the pdf expression in (16) is not in a compact analytical form and it does not seem to be possible to invert it to obtain parameter values, we employ a Bayesian sampling methodology in order to estimate model parameters. In this section, a Markov chain Monte Carlo (MCMC) based method is developed for estimating GG-Rician distribution parameters, namely the shape parameter  $\alpha$ , the scale parameter  $\gamma$ , and the location parameter  $\delta$ . In particular, the method uses the Metropolis-Hastings (MH) algorithm, and in each iteration, it applies one of three different moves:

- 1)  $\mathcal{M}_1$  which updates  $\delta$  for fixed  $\alpha$  and  $\gamma$ ,
- 2)  $\mathcal{M}_2$  which updates  $\gamma$  for fixed  $\alpha$  and  $\delta$ ,
- 3)  $\mathcal{M}_3$  which updates  $\alpha$  for fixed  $\gamma$  and  $\delta$ .

The proposed parameter estimation procedure is given in Algorithm 1. Given the observed data  $y$ , the hierarchical model is expressed by Bayes' theorem as

$$p(\alpha, \delta, \gamma|y) \propto p(y|\alpha, \delta, \gamma)p(\alpha)p(\gamma)p(\delta) \quad (34)$$

where  $p(\alpha, \delta, \gamma|y)$  is the joint posterior distribution, or the MH target distribution,  $p(y|\alpha, \delta, \gamma)$  refers to the likelihood distribution, and  $p(\alpha)$ ,  $p(\gamma)$  and  $p(\delta)$  are the priors.

Due to lack of knowledge on conjugate priors, we choose non-informative priors for the shape, location and scale (Jeffrey's) parameters. In particular, we assume that the location and shape parameters  $\alpha$  and  $\delta$  are uniformly distributed and that the prior for the scale parameter  $\gamma$  is  $p(\gamma) = 1/\gamma$ , which lead to  $p(\alpha, \delta, \gamma) \sim 1/\gamma$ . The likelihood  $p(y|\alpha, \delta, \gamma)$  is the GG-Rician distribution in (16) with parameters  $\alpha$ ,  $\gamma$  and  $\delta$ .

Depending on the selected move in iteration  $i$ , one of the proposal distributions given below is used to sample candidate parameters  $\delta^*$ ,  $\gamma^*$  or  $\alpha^*$

$$\mathcal{M}_1 : \delta^* \propto q(\delta^*|\delta^{(i)}) = \mathcal{U}(\delta^{(i)} - \epsilon, \delta^{(i)} + \epsilon), \quad (35)$$

$$\mathcal{M}_2 : \gamma^* \propto q(\gamma^*|\gamma^{(i)}) = \mathcal{N}(\gamma^{(i)}, \xi^2), \quad (36)$$

$$\mathcal{M}_3 : \alpha^* \propto q(\alpha^*|\alpha^{(i)}) = \mathcal{U}(\alpha^{(i)} - \eta, \alpha^{(i)} + \eta), \quad (37)$$

where  $\mathcal{U}(\cdot)$  is the uniform, and  $\mathcal{N}(\cdot)$  is the Gaussian distributions, both of which are defined in the interval  $[0, \infty]$  since  $\alpha$ ,  $\delta$  and  $\gamma$  are positive parameters.  $\eta$ ,  $\epsilon$  and  $\xi$  are hyper-parameters of the proposal distributions. Please note that these selection of proposals are not unique and can be replaced with any other distribution for better performance in estimating model parameters, faster convergence, etc.

### Algorithm 1 MCMC Parameter Estimation for GG-Rician Distribution

---

```

1: Inputs: Given data  $y$ .
2: Output: Joint Posterior  $f(\alpha, \delta, \gamma|y)$ 
3: Initialise:  $\alpha^{(1)}$ ,  $\delta^{(1)}$ ,  $\gamma^{(1)}$ ,  $\eta$ ,  $\nu$  and  $\xi$ .
4: for  $i = 1 : N_{iter}$  do
5:   Choose Move,  $m^{(i)}$  equally likely between  $\mathcal{M}_1$ ,  $\mathcal{M}_2$  or  $\mathcal{M}_3$ 
6:   if  $m^{(i)} \rightarrow \mathcal{M}_1$  then
7:     Sample  $\delta^* \sim q(\delta^*|\delta^{(i)})$ 
8:     Set  $\alpha^* = \alpha^{(i)}$  and  $\gamma^* = \gamma^{(i)}$  and  $A = A_{\mathcal{M}_1}$ .
9:   elseif  $m^{(i)} \rightarrow \mathcal{M}_2$  then
10:    Sample  $\gamma^* \sim q(\gamma^*|\gamma^{(i)})$ 
11:    Set  $\alpha^* = \alpha^{(i)}$  and  $\delta^* = \delta^{(i)}$  and  $A = A_{\mathcal{M}_2}$ .
12:   elseif  $m^{(i)} \rightarrow \mathcal{M}_3$  then
13:     Sample  $\alpha^* \sim q(\alpha^*|\alpha^{(i)})$ 
14:     Set  $\delta^* = \delta^{(i)}$  and  $\gamma^* = \gamma^{(i)}$  and  $A = A_{\mathcal{M}_3}$ .
15:   end if
16:   Sample random variable  $u \sim \mathcal{U}(0, 1)$ 
17:   if  $u \leq A$  then
18:      $\alpha^{(i+1)} = \alpha^*$  and  $\delta^{(i+1)} = \delta^*$  and  $\gamma^{(i+1)} = \gamma^*$ 
19:   else
20:      $\alpha^{(i+1)} = \alpha^{(i)}$  and  $\delta^{(i+1)} = \delta^{(i)}$  and  $\gamma^{(i+1)} = \gamma^{(i)}$ 
21:   end if
22: end for

```

---

Consequently, the acceptance probability expressions for each move can be expressed as

$$A_{\mathcal{M}_1} = \min \left( 1, \frac{p(y|\alpha^*, \delta^*, \gamma^*)q(\delta^{(i)}|\delta^*)}{p(y|\alpha^{(i)}, \delta^{(i)}, \gamma^{(i)})q(\delta^*|\delta^{(i)})} \right), \quad (38)$$

$$A_{\mathcal{M}_2} = \min \left( 1, \frac{p(y|\alpha^*, \delta^*, \gamma^*)p(\gamma^*)q(\gamma^{(i)}|\gamma^*)}{p(y|\alpha^{(i)}, \delta^{(i)}, \gamma^{(i)})p(\gamma^{(i)})q(\gamma^*|\gamma^{(i)})} \right), \quad (39)$$

$$A_{\mathcal{M}_3} = \min \left( 1, \frac{p(y|\alpha^*, \delta^*, \gamma^*)q(\alpha^{(i)}|\alpha^*)}{p(y|\alpha^{(i)}, \delta^{(i)}, \gamma^{(i)})q(\alpha^*|\alpha^{(i)})} \right). \quad (40)$$

### IV. EXPERIMENTAL ANALYSIS

The proposed method was tested from four different perspectives using both simulated and real data.

- 1) In the first simulation case, we used synthetically generated GG-Rician data for various parameters and tested the parameter estimation performance of the proposed MCMC method.
- 2) Second, we subsequently conducted experiments to determine the best fitting amplitude distribution for given real SAR images of various scenes.
- 3) Third, we evaluated the estimated GG-Rician model parameters on a large SAR scene, which was then decomposed into several image patches of  $250 \times 250$ . For each patch, estimated model parameters are combined

TABLE II  
MODELLING AND STATISTICAL SIGNIFICANCE RESULTS FOR SYNTHETICALLY GENERATED GG-RICIAN DATA SETS.

$(\alpha, \delta, \gamma)$	Est. Shape* ( $\hat{\alpha}$ )	Est. Location* ( $\hat{\delta}$ )	Est. Scale* ( $\hat{\gamma}$ )	KL Div.	KS Score
(1.7, 2.9, 2.3)	1.58±0.111	2.74±0.040	2.26±0.129	0.0043	0.0194
(1.45, 1, 5)	1.42±0.081	1.09±0.391	4.97±0.342	0.0049	0.0158
(1.1, 10, 2)	1.04±0.043	10.09±0.051	1.86±0.118	0.0069	0.0112
(0.7, 5, 1.5)	0.79±0.022	4.86±0.091	1.98±0.133	0.0137	0.0321
(1.2, 47, 32)	1.31±0.078	46.74±0.787	34.92±2.207	0.0042	0.0191
(0.5, 2, 0.5)	0.59±0.032	2.00±0.086	0.94±0.186	0.0153	0.0468
(1, 1.7, 1.3)	1.04±0.038	1.71±0.035	1.39±0.081	0.0018	0.0134
(2, 2, 4)	1.85±0.151	2.05±0.163	3.73±0.242	0.0032	0.0079

\* Estimated values are given in a format of: (posterior mean)±(posterior standard deviation).

to create a parameter map, which potentially gives ideas on how the different parts of a large image effects the estimated parameters of the GG-Rician model.

- 4) For the fourth and the last set of simulations, we performed a modelling study on intensity SAR images using the GG-Rician distribution.

We used the statistical significance measures of *Kullback-Leibler* (KL) divergence, *Kolmogorov-Smirnov* (KS) score in order to assess the performance of fitting distributions. Smaller KL and KS values indicates a better modelling performance. KL divergence is used to test the performance by considering the estimated pdfs and data histograms, whereas KS score is calculated by evaluating the estimated and the empirical cumulative distribution functions (CDFs).

The number of iterations,  $N_{iter}$  in the MCMC parameter estimation method was set to 1000 and the first 500 iterations were discarded as burn-in period. Initial values for the parameters  $\alpha^{(1)}$ ,  $\delta^{(1)}$  and  $\gamma^{(1)}$  were set to 2, 10 and 10, respectively. For proposal hyper-parameters, we chose  $\epsilon = 2.5$ ,  $\xi = 3$ , and  $\eta = 0.5$  after a trial-error procedure. All three model moves  $\mathcal{M}_1$ ,  $\mathcal{M}_2$  and  $\mathcal{M}_3$  are equiprobable whilst satisfying  $p(\mathcal{M}_1) + p(\mathcal{M}_2) + p(\mathcal{M}_3) = 1$ . For all state-of-the-art statistical models, we utilised an MCMC based maximum likelihood (ML) methodology to estimate the model parameters. The number of histogram bins for analysis was calculated for each image by using Sturge's method [25].

#### A. Synthetically Generated Data

In the first set of simulations, eight synthetically generated GG-Rician data sets were obtained and the proposed parameter estimation method was used to estimate  $\alpha$ ,  $\delta$  and  $\gamma$  for each data set. The corresponding data sets were generated for  $(\alpha, \delta, \gamma)$  which are given in Table II. Each data set has 1500 samples, and the results are presented in Table II and Figure 2.

By examining estimated values in Table II, we can clearly see that all the model parameters  $\alpha$ ,  $\gamma$  and  $\delta$  are correctly estimated and are very close to their true values. For all eight example data sets, statistical significance values are obviously low which certifies that the model parameters are successfully estimated.

Figure 2 shows modelling and parameter estimation results for the synthetically generated data from GG-Rician model

of (1, 1.7, 1.3). When examining sub-figures in Figure 2-(a) and (b), we can obviously state that the fitted distribution follows the generated data histogram well for both numerical and logarithmic scales. Sub-figures in Figure 2-(c)-(e) show instantaneous estimates for the parameters  $\alpha$ ,  $\delta$  and  $\gamma$ , respectively. The vertical line in all sub-figures represent the burn-in period, whilst the black and pink lines refer to the true and posterior mean values of the model parameters. When examining sub-figures in Figure 2-(c)-(e), we can clearly state that the parameter estimation method converges to the true parameter values within  $N_{iter}$  iterations. Furthermore, 500 iterations of burn-in period looks like a good choice since all instantaneous estimates are scattered around the true model parameters after the burn-in period.

#### B. Real Amplitude SAR Data

In the second set of simulations, the proposed method was tested for 43 different SAR images coming from various platforms with frequency bands of *X* (TerraSAR-X, COSMO-SkyMed and ICEYE), *L* (ALOS-2) and *C* (Sentinel-1). Each SAR image corresponds to one type of scene investigate, i.e. *urban*, *agricultural*, *mountain*, *land cover*, *mixed* and *sea surface with and without ships and their wakes*. Since we have three sources for X band SAR imagery as mentioned above, we have more X band example images in this study, the exact distribution of images in terms of scenes and frequency bands is given in Table III.

TABLE III  
DISTRIBUTION OF IMAGES IN TERMS OF SCENE AND FREQUENCY BANDS.

Scene	Frequency band			Total
	X	C	L	
Urban	4	3	0	7
Agricultural	3	3	2	8
Land	4	1	1	6
Mountain	1	2	3	6
wS/Sea	3	1	1	5
woS/Sea	2	2	1	5
Mixed	2	3	1	6
Total	19	15	9	43

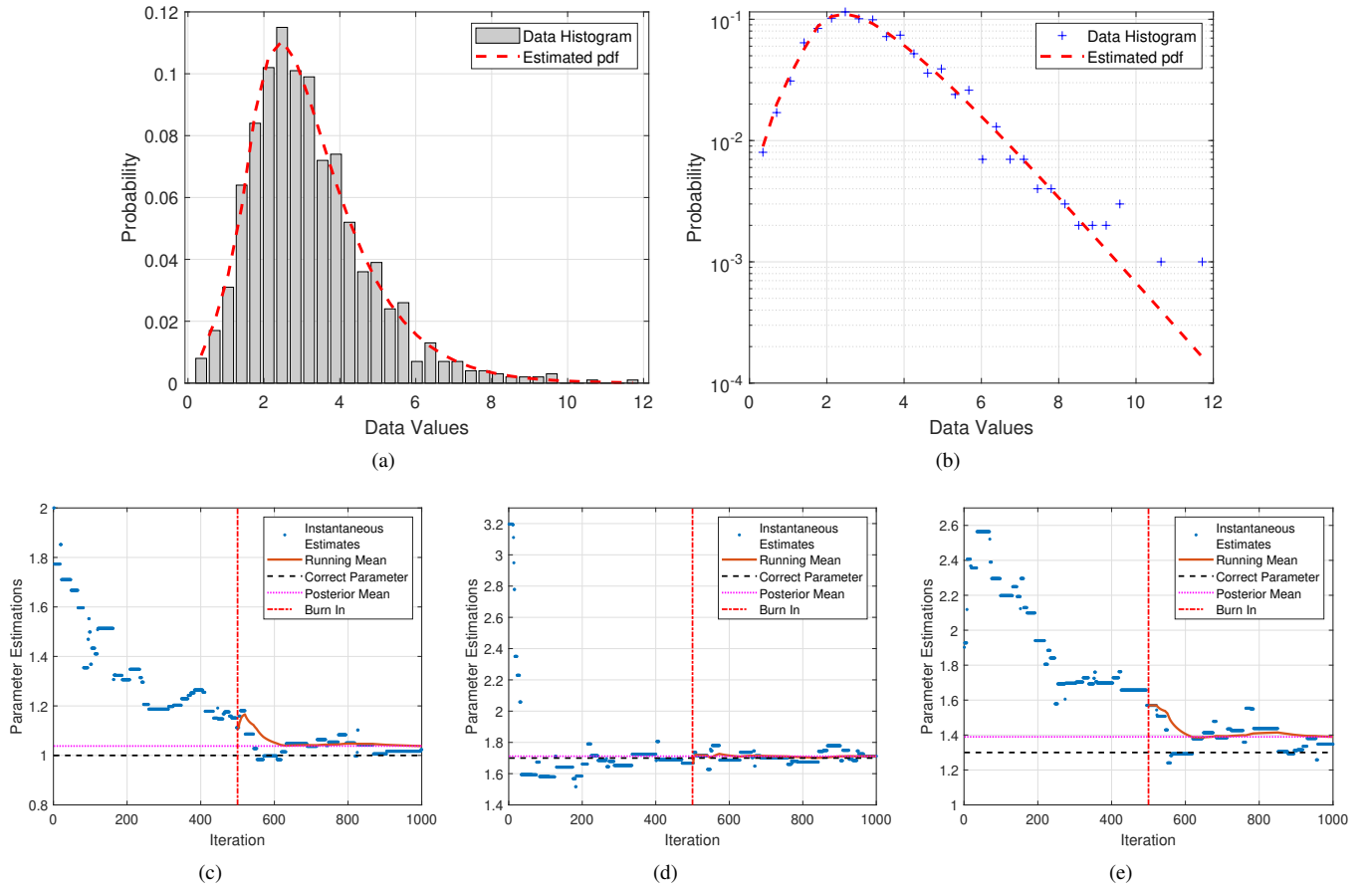


Fig. 2. Modelling and parameter estimation results for synthetically generated data for the GG-Rician model of (1, 1.7, 1.3). (a) pdf Fitting. (b) Log-pdf fitting. Instantaneous estimates are presented for (c) The shape parameter  $\alpha$ , (d) The location parameter  $\delta$ , and (e) The scale parameter  $\gamma$ .

Initially, each utilised SAR image was down-sampled to have a sample size of around 8000-10000. The down-sampling factor was different for each image since images had various sizes. The modelling performance of the proposed statistical model was compared to state-of-the-art statistical models including  $\mathcal{K}$ , Rayleigh, Rician, Weibull, lognormal, SR [5] and GGR [6]. Finally, the corresponding modelling results are presented in Tables IV and V, and depicted in Figure 3. In order to prevent repeating similar results and conclusions, instead of sharing KL and KS values specifically for each image, in Tables IV and V, we shared the percentages of images, that models achieved the best performance in terms of KL or KS.

Modelling results in terms of KL divergence and KS score for all 43 SAR images utilised in this paper are presented on the first rows of Tables IV and V, respectively. This statistical significance analysis clearly shows that for around 60% and 81% of the images respectively for KL and KS scores, the most suitable distribution to model SAR amplitude images of different scenes is the proposed GG-Rician distribution. When examining the scene specific statistical significance results in terms of KL divergence in Table IV, we can obviously state that for each of the utilised SAR scenes, the GG-Rician model achieves the best performance results by being most suitable model for more (or at least equal number of) images than the

second best statistical model. On the other hand, Lognormal model also shows a good modelling performance for urban and mountain scenes by achieving the best modelling results for the same number of images like the proposed model in terms of KL divergence. For the scene specific KS scores presented in Table V, for all the scenes utilised in this paper, the GG-Rician model achieves the smallest KS Score values for more images than the second best model, which leads the GG-Rician to have the best modelling results.

When we examine the frequency band specific performance analysis results in terms of KL divergence given in Table IV, For X and C band SAR amplitude images, the GG-Rician model shows the best modelling performance for most of the images, whereas for L band, Lognormal appears to be the best model overall scenes. For the KS score performance results presented in Table V, for all the frequency bands, the GG-Rician becomes the most suitable statistical model.

Figure 3 presents SAR images for six different scenes and their modelling results in logarithmic scale. The log-scale pdf modelling results in Figure 3 confirm the numerical results presented in Tables IV and V, whereby the GG-Rician model outperforms the most of the reference models utilised in this study and follows the data histograms better than the others.

In all the statistical significance results presented in Tables IV and V, despite being the best model over all images, it

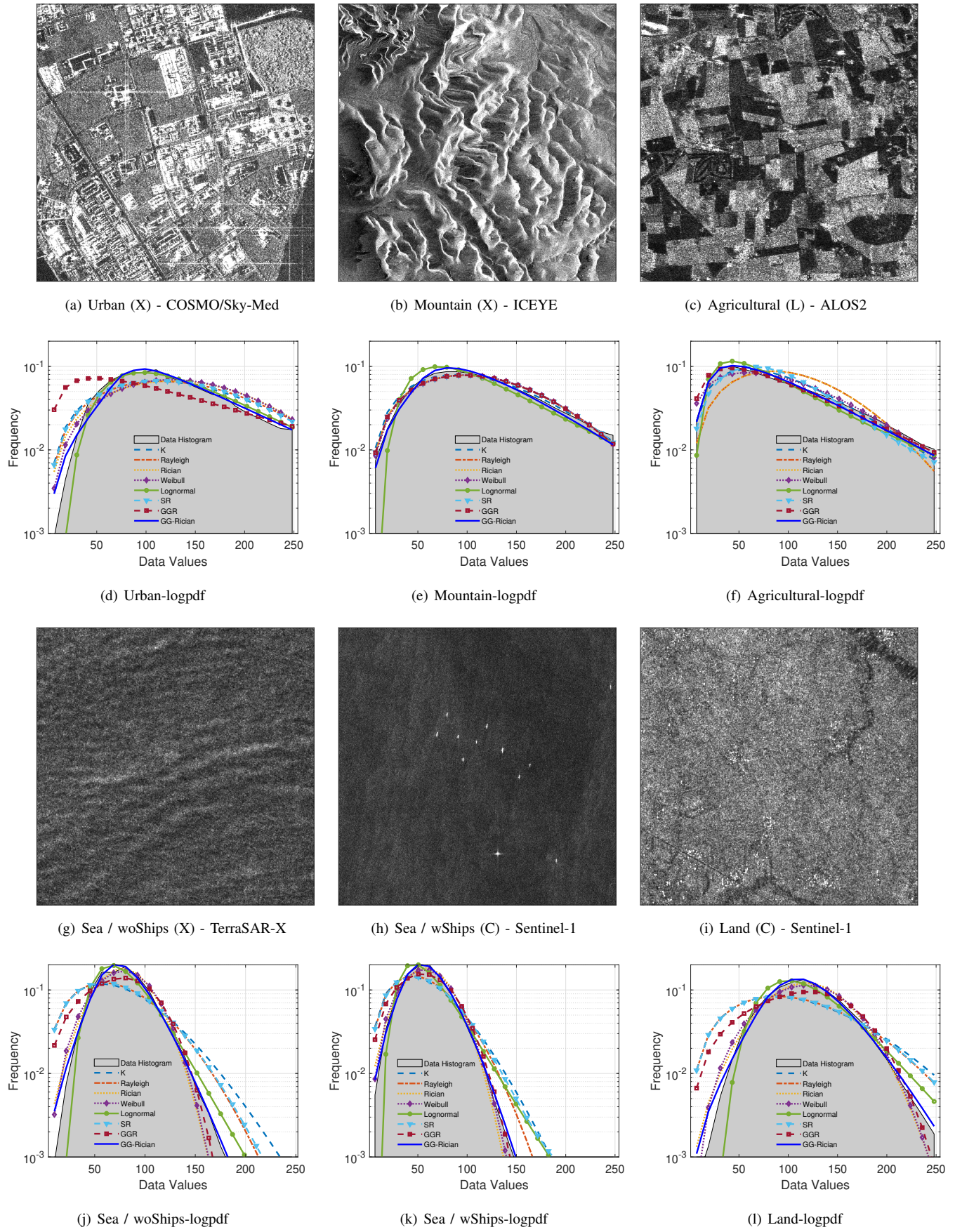


Fig. 3. Visual evaluation of SAR amplitude models.

TABLE IV  
MODELLING PERFORMANCE IN TERMS OF KL DIVERGENCE.

	$\mathcal{K}$	Rayleigh	Rician	Weibull	Lognormal	GGR	SR	GG-Rician
Overall	0.00%	0.00%	0.00%	4.65%	34.88%	0.00%	0.00%	<b>60.47%</b>
Scene	Urban	0.00%	0.00%	0.00%	14.29%	<b>42.86%</b>	0.00%	0.00%
	Agricultural	0.00%	0.00%	0.00%	37.50%	0.00%	0.00%	<b>62.50%</b>
	Mountain	0.00%	0.00%	0.00%	<b>50.00%</b>	0.00%	0.00%	<b>50.00%</b>
	Land	0.00%	0.00%	0.00%	16.67%	33.33%	0.00%	<b>50.00%</b>
	Mixed	0.00%	0.00%	0.00%	16.67%	0.00%	0.00%	<b>83.33%</b>
	wS/Sea	0.00%	0.00%	0.00%	40.00%	0.00%	0.00%	<b>60.00%</b>
	woS/Sea	0.00%	0.00%	0.00%	20.00%	0.00%	0.00%	<b>80.00%</b>
Freq. Band	X	0.00%	0.00%	0.00%	10.53%	31.58%	0.00%	0.00%
	C	0.00%	0.00%	0.00%	26.67%	0.00%	0.00%	<b>73.33%</b>
	L	0.00%	0.00%	0.00%	<b>55.56%</b>	0.00%	0.00%	44.44%

TABLE V  
MODELLING PERFORMANCE IN TERMS OF KS SCORE.

	$\mathcal{K}$	Rayleigh	Rician	Weibull	Lognormal	GGR	SR	GG-Rician
Overall	2.33%	0.00%	0.00%	6.98%	11.63%	0.00%	0.00%	<b>81.40%</b>
Scene	Urban	0.00%	0.00%	0.00%	14.29%	28.57%	0.00%	0.00%
	Agricultural	12.50%	0.00%	0.00%	0.00%	12.50%	0.00%	0.00%
	Mountain	0.00%	0.00%	0.00%	0.00%	16.67%	0.00%	0.00%
	Land	0.00%	0.00%	0.00%	33.33%	0.00%	0.00%	<b>66.67%</b>
	Mixed	0.00%	0.00%	0.00%	0.00%	0.00%	0.00%	<b>100.00%</b>
	wS/Sea	0.00%	0.00%	0.00%	0.00%	20.00%	0.00%	0.00%
	woS/Sea	0.00%	0.00%	0.00%	0.00%	0.00%	0.00%	<b>100.00%</b>
Freq. Band	X	5.26%	0.00%	0.00%	15.79%	5.26%	0.00%	0.00%
	C	0.00%	0.00%	0.00%	0.00%	20.00%	0.00%	0.00%
	L	0.00%	0.00%	0.00%	0.00%	11.11%	0.00%	0.00%

is clearly seen that KL divergence results for the GG-Rician model is somehow worse than that of KS scores. In order to analyse the reason behind this performance, we show two examples in Figure 4. The example comparison plot in Figure 4-(a) shows a modelling case where the Lognormal model achieves the best modelling results in terms of KL divergence values, whilst for the KS score the GG-Rician model is the best statistical model. Figure 4-(b) shows a modelling case where the GG-Rician model achieves the best modelling results in terms of the both statistical measures. When examining Figure 4-(a), for the data points in the rectangle, GG-Rician fails to follow the data points where Lognormal shows a closer fit. The main reason for GG-Rician model to have worse modelling results in terms of KL values is the limited amount of low amplitude pixels as shown in the example, hence the estimate being rough. Despite its worse fit for the left (lower amplitude pixels) tail of the data histogram, GG-Rician provides a better model for the data values around the peak value (high probability region in ellipse) and the right tail (higher amplitude pixels). Since KL scales the weights according to the relative entropy while KS looks at the cumulative distribution, these low amplitude areas with small number of pixels seems to have affected the results unevenly.

In order to give an example to support this reasoning and counter to the average KL results, we depict the Figure 4-(b).

We can clearly state that when compared to the SAR data in Figure 4-(a), data has higher probabilities for dark (low-amplitude) pixels than the bright (high-amplitude) ones, which is better described by the GG-Rician model in both tails and the main lobe. However, we can clearly see that the Lognormal model fails to model both tails and the higher probability region at the same time. This characteristic of the proposed GG-Rician model provides the reason why the proposed model is having difficulties to have lower KL divergence values for the urban and the mountain scenes (see Table IV), which are generally bright and obtain less darker radar returns. Finally, the same effects in Figure 4-(a) and (b) can also be seen in Figure 3-(d) and (f).

### C. Analysis on Estimated GG-Rician Model Parameters

In the third set of simulations, we analysed estimated GG-Rician model parameters, and their variations depending on the different surface characteristics in a single large SAR scene.

We chose two example amplitude SAR images, each of which are TerraSAR-X products for sea surface with and without ships, and their corresponding wakes (Figure 5-(a) and (b)). We believe that SAR images of this type include several distinct structures, such as land/mountain, urban area, sea, ships, shorelines, some islands, and even agricultural, which are suitable for the analysis in this simulation case. Each large

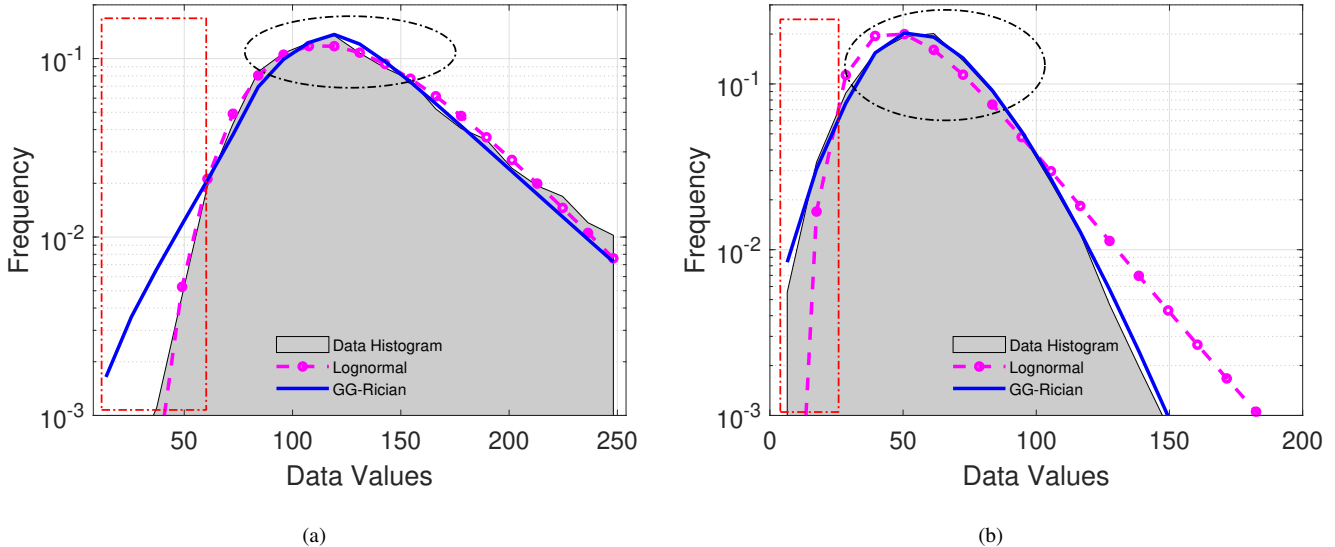


Fig. 4. A direct comparison between the GG-Rician and Lognormal models for two different cases. (a) The best in terms of KL Div. is Lognormal, whilst in terms of KS, GG-Rician is the best model. (b) GG-Rician is the best for KL and KS measures.

image were decomposed into  $250 \times 250$  pixel patches and each patch was modelled via the proposed GG-Rician model. For each patch, we estimated model parameters and we plot them as images in Figure 5-(c)-(h).

When examining shape parameter estimations for both images, we could state that areas including bright radar returns such as mountain tops, buildings, have relatively high shape parameter estimates, e.g. around  $\alpha$  estimates of 2-3. For the sea surface, we can conclude that the shape parameter estimates do not directly reflect the changes of the sea surface, the estimated values of which generally lie around 1-2.

In Figures 5-(d) and (g), we show the location parameter delta estimates for two example images. When examining these sub-figures, we can obviously state that the location parameter estimates reflect a direct relation with the original image amplitude values, and provide a so-called good "down-sampled version" of the original image. Different wave heights, shore-lines, as well as bright amplitudes such as urban areas are clearly distinguishable. We believe that as a feature, the location parameter  $\delta$  of the proposed model would play an important role in classification examples regarding the amplitude SAR images.

The estimated scale parameters for each patch are depicted in Figure 5-(e) and (h). Both sub-figures generally show similar characteristics to the shape parameter estimates. For bright radar returns, it takes a  $\gamma$  of around 100-140. The sea and land regions can be easily distinguished between them according to the estimated scale parameter value, whilst the sea surface changes are not distinguishable from the  $\gamma$  estimates.

Please note that, different from most of the statistical models, the GG-Rician model includes a location parameter. As a remark of this analysis, we can state that it is the most suitable parameter to reflect the radical changes on the SAR scene, and can be shown as an important advantage of the proposed statistical model, specifically in applications such as segmentation, classification.

#### D. Real Intensity SAR Data

In the fourth and the last simulation case, we evaluated the performance of the intensity GG-Rician model. For this simulation case, we only utilised three example intensity SAR images. We left the further analysis of the intensity model as future work.

The same procedure for the amplitude SAR modelling was also applied here for the intensity images. The same parameter estimation methodology was used to estimate the model parameters of the intensity GG-Rician model. For the reference models, in addition to  $\mathcal{K}$  and Weibull (thanks to their intensity modelling capabilities), the Gamma distribution was also used.

TABLE VI  
STATISTICAL SIGNIFICANCE FOR INTENSITY SAR IMAGE MODELLING

Image	Stats	$\mathcal{K}$	Weibull	Gamma	GG-Rician
wS/Sea	KL Div	0.0767	0.0756	<b>0.0133</b>	0.0154
	KS Score	0.0690	0.0564	0.0301	<b>0.0181</b>
Mixed	KL Div	0.0358	0.0755	0.0365	<b>0.0064</b>
	KS Score	0.0740	0.0867	0.0697	<b>0.0297</b>
Urban	KL Div	0.5484	0.1084	0.1622	<b>0.0144</b>
	KS Score	0.3383	0.1715	0.2117	<b>0.0512</b>

The corresponding results are depicted in Figure 6, and statistical significance of modelling is given in Table VI. There are three SAR images of scenes: Sea with ships, Mixed and Urban, respectively in Figure 6-(a), (b) and (c). The

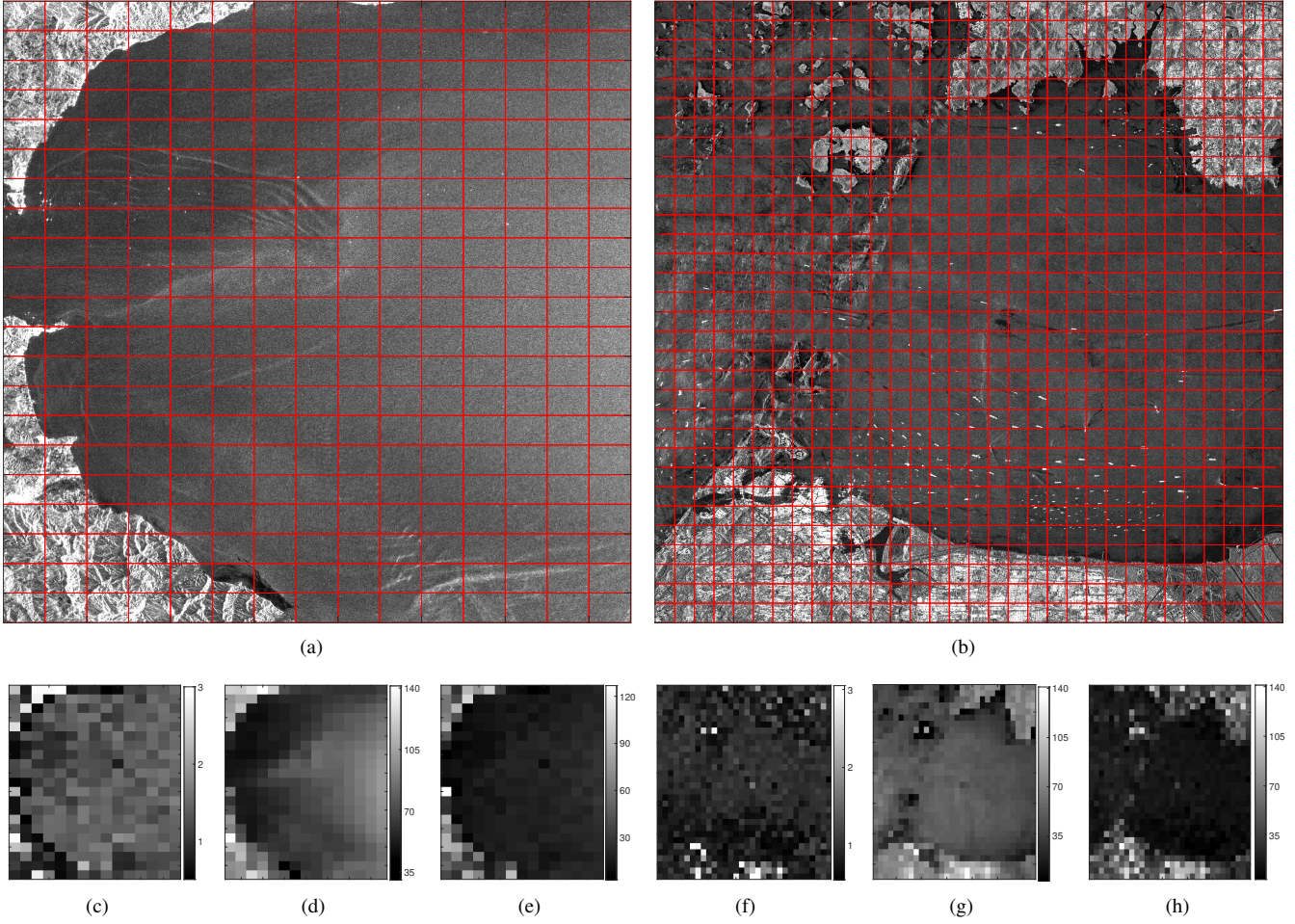


Fig. 5. Estimated model parameters for two large SAR scenes for  $250 \times 250$  image patches in red rectangles. (a) Original Image-1 ( $5250 \times 3750$ ). (b) Original Image-2 ( $8000 \times 8000$ ). (c) and (f) The shape parameter  $\alpha$ . (d) and (g) The location parameter  $\delta$ . (e) and (h) The scale parameter  $\gamma$ .

corresponding modelling results are presented in logarithmic scale in sub-figures from (d) to (f). The superior modelling performance of the proposed GG-Rician intensity model compared to the state-of-the-art models is obvious.

## V. CONCLUSIONS

In this paper, we proposed a novel parametric statistical model, namely the GG-Rician model, to characterise the amplitude and the intensity of the complex back-scattered SAR signal. Specifically, the GG-Rician model is an extension of Rician model whereby the Gaussian components of the complex SAR signal are replaced by the generalised-Gaussian distribution. A closed form pdf expression in integral form was derived and a Bayesian sampling scheme for the model parameter estimation was developed. We have tested the modelling performance of the GG-Rician model both for synthetically generated and real SAR data, which are specifically coming from satellite platforms of TerraSAR-X, Sentinel-1, ICEYE, COSMO/Sky-Med and ALOS2.

The performance of the proposed statistical model was then compared to the state-of-the-art statistical models of  $\mathcal{K}$ , Rician, Rayleigh, Weibull, Lognormal, SR, GGR and Gamma. The results demonstrate that the proposed method

achieves the best modelling results for most of the images, and outperforms state-of-the-art models for images from various frequency bands and sources. It is interesting to note that the results show us the need for combining the advantages of non-Gaussian heavy-tailed modelling and non-zero mean reflections modelling provided by Rician model. That is quite obvious when we compare Laplace-Rician with  $\mathcal{K}$ , SR, GGR, Rician and Rayleigh directly. Furthermore, using non-zero reflections along with the heavy-tailed modelling in GG-Rician model shows important success in all types of SAR scenes and frequency bands.

In all the experimental analyses in this paper, we have experienced that the extension of the idea of having GG-distributed components, from Rayleigh (zero-mean components) to Rician (non-zero mean components) demonstrated a great success when compared to its Rayleigh counterpart GGR [6]. For all types of scenes and frequency bands, the GG-Rician model outperformed GGR model. On the other hand, please note that since the GGR model is actually a simplified special member (for  $\delta = 0$ ) of the proposed GG-Rician model, we can conclude that we successfully strengthened GGR to a more flexible and robust model by covering various different characteristics. It is also very clear to state that the gain

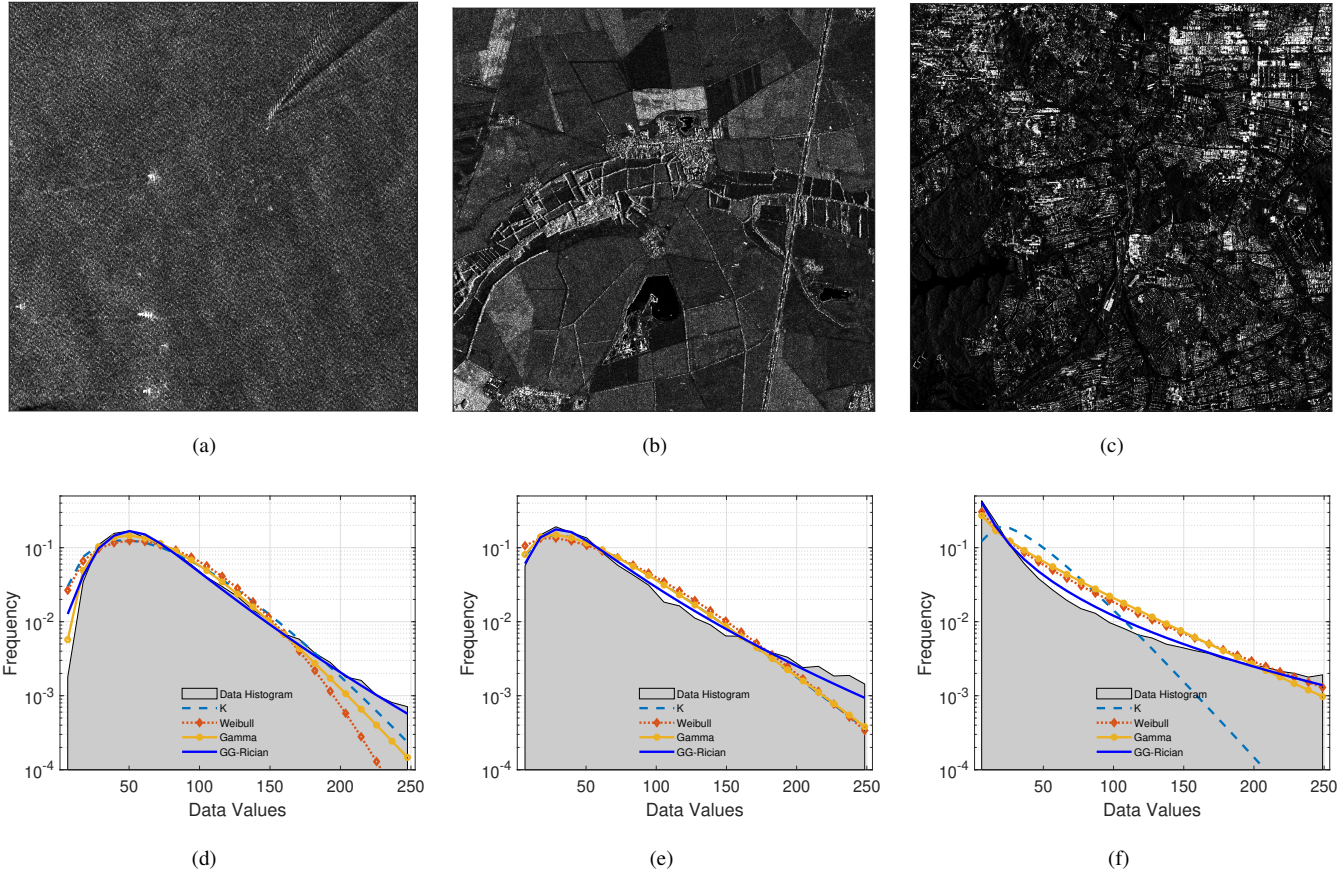


Fig. 6. Intensity modelling comparison. Intensity SAR images from scenes of (a) sea with ships, (b) mixed, and (c) urban . Sub-figures in (d)-(f) refer to the corresponding modelling results in log-pdf scale for intensity images in (a)-(c), respectively.

with using non-Gaussian components over the classical Rician model is obvious. The flexibility of adjusting tails (via a shape parameter) in conjunction with the location parameter demonstrated a remarkable gain over the Rician model for all the simulation cases which are demonstrated in this paper. Our future work will investigate developing faster parameter estimation methods.

#### ACKNOWLEDGMENT

We are grateful to the UK Satellite Applications Catapult for providing us the COSMO-SkyMed data sets employed in this study.

#### REFERENCES

- [1] C. Tison, J.-M. Nicolas, F. Tupin, and H. Maître, “A new statistical model for Markovian classification of urban areas in high-resolution SAR images,” *IEEE transactions on Geoscience and Remote Sensing*, vol. 42, no. 10, pp. 2046–2057, 2004.
- [2] M. E. Mejail, J. C. Jacobo-Berilles, A. C. Frery, and O. H. Bustos, “Classification of SAR images using a general and tractable multiplicative model,” *International Journal of Remote Sensing*, vol. 24, no. 18, pp. 3565–3582, 2003.
- [3] A. Achim, E. E. Kuruoglu, and J. Zerubia, “SAR image filtering based on the heavy-tailed Rayleigh model,” *IEEE Transactions on Image Processing*, vol. 15, no. 9, pp. 2686–2693, 2006.
- [4] F. Argenti, A. Lapini, T. Bianchi, and L. Alparone, “A tutorial on speckle reduction in synthetic aperture radar images,” *IEEE Geoscience and Remote Sensing magazine*, vol. 1, no. 3, pp. 6–35, 2013.
- [5] E. E. Kuruoglu and J. Zerubia, “Modeling SAR images with a generalization of the Rayleigh distribution,” *IEEE Transactions on Image Processing*, vol. 13, no. 4, pp. 527–533, 2004.
- [6] G. Moser, J. Zerubia, and S. B. Serpico, “SAR amplitude probability density function estimation based on a generalized Gaussian model,” *IEEE Transactions on Image Processing*, vol. 15, no. 6, pp. 1429–1442, 2006.
- [7] M. D. DeVore, A. D. Lanterman, and J. A. O’Sullivan, “ATR performance of a Rician model for SAR images,” in *Automatic Target Recognition X*, vol. 4050. International Society for Optics and Photonics, 2000, pp. 34–45.
- [8] J. Sun, X. Wang, X. Yuan, Q. Zhang, C. Guan, and A. V. Babanin, “The Dependence of Sea SAR Image Distribution Parameters on Surface Wave Characteristics,” *Remote Sensing*, vol. 10, no. 11, p. 1843, 2018.
- [9] M. Migliaccio, L. Huang, and A. Buono, “Sar speckle dependence on ocean surface wind field,” *IEEE Transactions on Geoscience and Remote Sensing*, vol. 57, no. 8, pp. 5447–5455, 2019.
- [10] S. Chitrub, A. Houacine, and B. Sansal, “Statistical characterisation and modelling of SAR images,” *Signal Processing*, vol. 82, no. 1, pp. 69–92, 2002.
- [11] S. Cui, G. Schwarz, and M. Dateu, “A comparative study of statistical models for multilook sar images,” *IEEE Geoscience and Remote Sensing Letters*, vol. 11, no. 10, pp. 1752–1756, 2014.
- [12] S. Ishii, S. Sayama, and K. Mizutani, “Effect of Changes in Sea-Surface State on Statistical Characteristics of Sea Clutter with X-band Radar,” *Wireless Engineering and Technology*, vol. 2, pp. 175–183, 2011.
- [13] J. R. M. Fernández, “Estimation of the relation between Weibull sea clutter and the CA-CFAR scale factor,” *Revista Ingeniería*, vol. 25, no. 2, pp. 19–28, 2015.
- [14] Z. Chen, X. Liu, Z. Wu, and X. Wang, “The Analysis of Sea Clutter Statistics Characteristics Based on the Observed Sea Clutter of Ku-Band Radar,” in *2013 Proceedings of the International Symposium on Antennas & Propagation*, vol. 2. IEEE, 2013, pp. 1183–1186.
- [15] X. Xing, Z. Chen, H. Zou, and S. Zhou, “Statistical assessment of

- model fit for SAR sea clutter,” in *MIPPR 2009: Multispectral Image Acquisition and Processing*, vol. 7494. International Society for Optics and Photonics, 2009, p. 74940R.
- [16] O. Karakuş, E. E. Kuruoğlu, and M. A. Altinkaya, “Generalized Bayesian model selection for speckle on remote sensing images,” *IEEE Transactions on Image Processing*, vol. 28, no. 4, pp. 1748–1758, 2018.
- [17] O. Karakuş, E. E. Kuruoğlu, and A. Achim, “Modelling sea clutter in SAR images using Laplace-Rician distribution,” in *ICASSP 2020 - 2020 IEEE International Conference on Acoustics, Speech and Signal Processing (ICASSP)*, 2020, pp. 1454–1458.
- [18] J.-M. Nicolas and F. Tupin, “A new parameterization for the Rician distribution,” *IEEE Geoscience and Remote Sensing Letters*, 2019.
- [19] T. Eltoft, “The Rician inverse Gaussian distribution: a new model for non-Rayleigh signal amplitude statistics,” *IEEE Transactions on Image Processing*, vol. 14, no. 11, pp. 1722–1735, 2005.
- [20] J. W. Goodman, “Statistical properties of laser speckle patterns,” in *Laser speckle and related phenomena*. Springer, 1975, pp. 9–75.
- [21] G. Gao, “Statistical modeling of SAR images: A survey,” *Sensors*, vol. 10, no. 1, pp. 775–795, 2010.
- [22] W. Wu, H. Guo, and X. Li, “Man-made target detection in urban areas based on a new azimuth stationarity extraction method,” *IEEE Journal of Selected Topics in Applied Earth Observations and Remote Sensing*, vol. 6, no. 3, pp. 1138–1146, 2013.
- [23] L. Denis, F. Tupin, and X. Rondeau, “Exact discrete minimization for TV+ L<sub>0</sub> image decomposition models,” in *2010 IEEE International Conference on Image Processing*. IEEE, 2010, pp. 2525–2528.
- [24] R. A. Dana and D. L. Knepp, “The impact of strong scintillation on space based radar design ii: Noncoherent detection,” *IEEE transactions on aerospace and electronic systems*, no. 1, pp. 34–46, 1986.
- [25] H. A. Sturges, “The choice of a class interval,” *Journal of the American Statistical Association*, vol. 21, no. 153, pp. 65–66, 1926.